

---

# DRUG DISCOVERY SMILES-TO-PHARMACOKINETICS DIFFUSION MODELS WITH DEEP MOLECULAR UNDERSTANDING

---

**Bing Hu**

Computer Science  
University of Waterloo  
bingxu.hu@uwaterloo.ca

**Anita Layton**

Applied Mathematics  
University of Waterloo  
anita.layton@uwaterloo.ca

**Helen Chen**

School of Public Health Sciences  
University of Waterloo  
helen.chen@uwaterloo.ca

## ABSTRACT

Artificial intelligence (AI) is increasingly used in every stage of drug development. One challenge facing drug discovery AI is that drug pharmacokinetic (PK) datasets are often collected independently from each other, often with limited overlap, creating data overlap sparsity. Data sparsity makes data curation difficult for researchers looking to answer research questions in poly-pharmacy, drug combination research, and high-throughput screening. We propose Imagand, a novel SMILES-to-Pharmacokinetic (S2PK) diffusion model capable of generating an array of PK target properties conditioned on SMILES inputs. We show that Imagand-generated synthetic PK data closely resembles real data univariate and bivariate distributions, and improves performance for downstream tasks. Imagand is a promising solution for data overlap sparsity and allows researchers to efficiently generate ligand PK data for drug discovery research. Code is available at <https://github.com/bing1100/Imagand>.

## 1 Introduction

Generative AI is set to transform drug discovery, where it may cost \$2-3 billion dollars and 10-15 years to bring a single drug candidate to market [30]. Generative AI for high-throughput screening (HTS) of ligand candidates reduces drug development costs and is changing how ligands are designed and tested [41]. Initial success of drug discovery AI has been in drug repurposing [36, 50], drug-target interaction [33], drug response prediction [40], poly-pharmacy [61], and the generation of synthetic ligands and drug properties [25, 52]. Thus far, what has advanced drug discovery AI is a continued effort towards open data for training and testing [8, 17, 27].

Data collection for drug discovery through assay panels is expensive and time-consuming. Although there are clear advances toward standardization and dissemination of pre-clinical, clinical, and chemical datasets [27, 31, 37], challenges arise when merging and linking these datasets together [46]. Collected independently, drug discovery datasets often have limited overlap, which poses a challenge for researchers looking to answer research questions requiring data from multiple datasets. One notable example is the study of drug combinations and poly-pharmacy [46].

Recent advances in drug discovery AI have utilized Denoising Diffusion Probabilistic Models (DDPMs) [21], which yield a new class of diffusion models capable of generating ligand structures [18, 28, 52, 58]. Hu et al. [25] have shown that diffusion models can generate pharmacokinetic (PK) properties alongside the ligand diffusion pipeline with promising results. Multi-modal diffusion models such as Text-to-Image and Text-to-Video diffusion models have been demonstrated to generate high-quality photorealistic data [23, 44]. Azizi et al. [4] have also shown that synthetic data from diffusion models have improved performance in ImageNet classification tasks. Inspired by these advances, we propose Imagand, which can generate an array of 12 PK target properties from 10 PK datasets conditioned on learned SMILES embeddings. Specifically, our contributions are as follows:

- We propose Imagand, a novel multi-modal SMILES-to-Pharmacokinetic (S2PK) diffusion model capable of generating an array of target properties conditioned on learned SMILES embeddings.
- We develop a noise model that creates a prior distribution closer to the true data distribution, which makes training easier [52].

- We show that synthetic data generated from our Imagand model closely resembles the univariate and bivariate distributions of the real data and improves performance on downstream tasks.

Notably, Imagand generates dense synthetic data that overcomes the challenges of sparse PK datasets with limited overlap. Using Imagand, researchers can generate large synthetic PK assays over thousands of ligands to answer poly-pharmacy and drug combination research questions at a fraction of the cost of conducting *in vitro* or *in vivo* PK assay panels.

## 2 Background

Diffusion methods use families of probability distributions to model complex datasets for computationally tractable learning, sampling, inference and evaluation [18]. Denoising Diffusion Probabilistic Models (DDPM) [21] first systematically destroy the structure in the data through a forward process, and then in a reverse process, learn how to restore the structure in the data from noise. Recent literature has covered many advances in small-molecule generation using diffusion models [24, 26, 45, 52].

DDPMs can be combined with graph networks. Conditional Diffusion models are based on discrete Graph Structures (CDGS) and can be used to generate small-molecule graphs with similar distribution to real small-molecules [26]. Digress [52] combines graph transformers [16] and discrete diffusion [3] for molecular-conditioned small-molecule generation. Digress utilizes graph-level properties such as cycles, and spectral and molecular features to augment the input, improving training and sampling performance. Conditional generation has shown benefits for diffusion Text-to-Image and Text-to-Video models [23, 44]. In Text-to-Image and Text-to-Video models, learned embeddings from Large Language Models (LLMs) are utilized as input to lend deep language understanding to the diffusion models.

PK broadly describes what the body does to a drug regarding absorption (how the body absorbs the drug), bioavailability (the extent the active drug enters circulation), distribution (how the drug distributes in tissue), metabolism (how the body breaks down the drug), and excretion (how the drug is removed from the body). As issues related to PK properties are the primary drivers for compound attrition for small-molecule drug development [32], accurate PK computational tools are critical and have advanced in recent times [2, 11, 55]. Physiologically-based pharmacokinetics (PBPK) offers the modelling of PK properties using mathematical equations representing the human body [43]. PBPK rely on expensive *in-vitro* and *in-vivo* human and animal experiments and cannot be utilized in high-throughput screening across large numbers of ligands (10K to 100K drugs per day) [39].

Extending many PK properties across large arrays of ligands can be costly given the expense associated with data collection for drugs. Consequently, oftentimes only small sets of ligands can be feasibly tested for target property data collection studies, leading to minimal overlap between collected datasets [46]. This challenge poses barriers for scientists interested in answering research questions requiring data across multiple datasets, such as in poly-pharmacy and drug combination research.

## 3 Methodology

Imagand is a S2PK diffusion model conditioned on learned SMILES embeddings from SMILES encoder models to generate target PK properties. We utilize a typical diffusion process as formulated in Ho et al. [21] with only modifications to the choice of noise model to better capture distribution priors. In the following subsections, we describe each of these components in detail.

### 3.1 Pre-trained SMILES Encoder

S2PK diffusion models need powerful semantic SMILE encoders to capture the complexity of arbitrary chemical structure inputs. Given the sparsity and small size of PK datasets, encoders trained on specific SMILES-Pharmacokinetic pairs are infeasible [27]. Many transformer-based foundational models such as ChemBERTa [1, 9], SMILES-BERT [54], and MOLGPT [5] have been pre-trained to deeply understand molecular and chemical structures and properties. After pre-training, these foundational models can then be fine-tuned for various downstream molecular tasks. Language models trained on SMILES-only corpus, significantly larger than SMILES-Pharmacokinetic data, learn a richer and wider distribution of molecular and chemical structures.

We test SMILES embeddings from ChemBERTa [1], T5 [42], and DeBERTa [19] trained on SMILES-only corpora. We further test and compare embedding performance for SMILES embedding from ChemBERTa trained either on ZINC (100K molecules) [29] or PubChem (10M molecules) [31] SMILES corpora. All SMILES embedding models were collected through the Huggingface [57] Model Hub. As ChemBERTa, T5, and DeBERTa are all trained on a wide

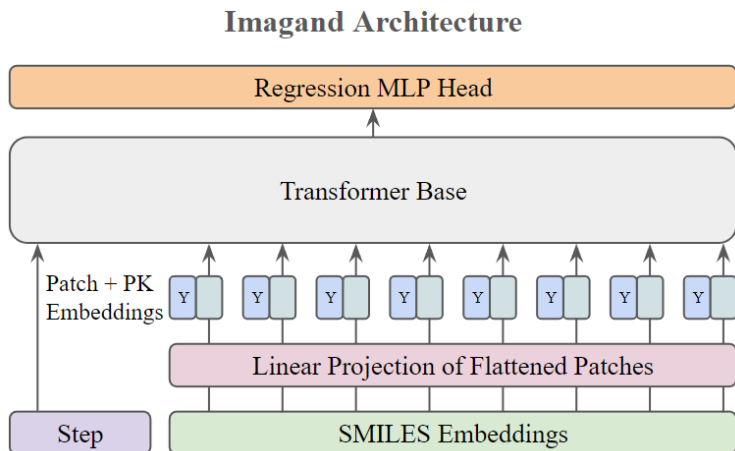


Figure 1: Model overview. Patches are generated from SMILES Embeddings combined with PK embeddings. The patches are then fed along with step embeddings into the base transformer model. A regression MLP head is used to produce the necessary output for denoising.

array of SMILES, embeddings from these models are an effective way to inject deep molecular understanding into our diffusion model. Similar to Saharia et al. [44], we freeze the weights of our embedding models. Because embeddings are computed offline, freezing the weights minimizes computation and memory footprint for embeddings during model training.

## 3.2 Diffusion Model

### 3.2.1 Base Model

Imagand resembles a typical vision transformer architecture [14]; see Figure 1. 1D patches are computed from the classifier-free guidance of SMILES embeddings and concatenated with PK class tokens. Diffusion step embeddings are generated using sinusoidal position encodings [51]. Patches are then fed alongside sinusoidal step embeddings [22] to a transformer base. We mask out missing values when computing the loss for the model only to flow gradients and learn from non-missing PK values during training. Exponential Moving Average (EMA) [49] is applied to the base model during training to generate the final model used for sampling.

### 3.2.2 Classifier-free Guidance

Classifier guidance uses gradients from a pre-trained model to improve quality while reducing diversity in conditional diffusion models during sampling [12]. Classifier-free guidance [20] is an alternative technique that avoids this pre-trained model by jointly training a diffusion model on conditional and unconditional objectives via dropping the condition (i.e. with 10% probability). We condition all diffusion models on learned SMILES embedding and sinusoidal time embeddings using classifier-free guidance through dropout [20, 48].

### 3.2.3 Static Thresholding

We apply elementwise clipping the PK predictions to  $[-1, 1]$  as static thresholding, similar to Ho et al. [21], Saharia et al. [44]. Since PK data is min-max scaled to the same  $[-1, 1]$  range as a preprocessing step, static thresholding is essential to prevent the generation of invalid and out-of-range PK values.

## 3.3 Discrete Local Gaussian Noise Model

The choice of noise models may have a substantial impact on performance; using a prior distribution close to the true data distribution can make training easier [52]. As PK properties do not always follow a Gaussian or uniform noise model, we propose a noise model called Discrete Local Gaussian Noise (DLGN). DLGN decomposes complex PK distributions as Gaussian distributions within discrete bins. Discrete bins are modelled as discrete random variables.

### 3.3.1 Discrete Bin Random Variables

Given a PK distribution, we first apply data binning to produce  $N$  bins. We define a discrete probability density function (PDF) on the bins, given in Equation 1, where  $X_i$  represents the set of PK values in bin  $i$ , where  $0 \leq i \leq N$ .

$$P(X_i) = \frac{|X_i|}{\sum_{j=0}^N |X_j|} \quad (1)$$

### 3.3.2 Local Gaussian Distribution

For each  $X_i$  bin, we define a Gaussian distribution  $\hat{X}_i$  as denoted in Equation 2 with mean and standard deviation computed from  $X_i$  bin.

$$\hat{X}_i \sim \mathcal{N}(\mu(X_i), \sigma^2(X_i)) \quad (2)$$

Once a bin  $X_j$  is chosen randomly from the discrete PDF (Equation 1), we then sample and return noise from the local bin Gaussian distribution  $\hat{X}_j$ . DLGN noise better resembles the prior distribution compared to Gaussian or uniform noise models, so training the model is faster.

## 3.4 Pharmacokinetic Datasets

All PK datasets are collected from TDCcommons [27]. We select PK datasets suitable for regression from the absorption, distribution, metabolism, and excretion (ADME) and Toxicity categories.

**Caco-2** [53] is an absorption dataset containing rates of 906 drugs passing through the Caco-2 cells, approximating the rate at which the drugs permeate through the human intestinal tissue. **Lipophilicity** [59] is an absorption dataset that measures the ability of 4,200 drugs to dissolve in a lipid (e.g. fats, oils) environment. **AqSolDB** [47] is an absorption dataset that measures the ability of 9,982 drugs to dissolve in water. **FreeSolv** [35] is an absorption dataset that measures the experimental and calculated hydration-free energy of 642 drugs in water.

**Plasma Protein Binding Rate (PPBR)** [56] is a distribution dataset of percentages for 1,614 drugs on how they bind to plasma proteins in the blood. **Volume of Distribution at steady state (VDss)** [34] is a distribution dataset that measures the degree for 1,130 drugs on their concentration in body tissue compared to their concentration in blood.

**Half Life** [38] is an excretion dataset for 667 drugs on the duration for the concentration of the drug in the body to be reduced by half. **Clearance** [13] is an excretion dataset for around 1,050 drugs on two clearance experiment types, microsome and hepatocyte. Drug clearance is defined as the volume of plasma cleared of a drug over a specified time [27].

**Acute Toxicity (LD50)** [60] is a toxicity dataset that measures the most conservative dose for 7,385 drugs that can lead to lethal adverse effects. **hERG Central** [15] is a toxicity dataset that measure the blocking of Human ether-à-go-go related gene (hERG) for 306,893 drugs. hERG is crucial for the coordination of the heart’s beating. hERG contains percentages inhibitions at  $1\mu M$  and  $10\mu M$ .

## 3.5 Data Processing

We first merge all 10 PK datasets to create a unified dataset containing 30K drugs over 12 unique PK columns for training and testing (90%/10% split) our models. Excluding the hERG dataset from which we sample 7.9K drugs, we merge the remaining 9 PK datasets for 22.1K unique drugs. We arrive at a total of 30K drugs in our unified dataset after merging the 7.9K drugs sampled from hERG into our 22.1K unique drugs from the other 9 PK datasets. We only sample 7.9K drugs from hERG to maintain balance in the unified dataset given the size imbalance of hERG compared to the other 9 PK datasets. After removing outliers ( $Q1 - 1.5IQR$  lower and  $Q3 + 1.5IQR$  upper bound), we are left with 28,397 drugs from the original 30K drugs. The 28,397 drug values for each of the 12 PK columns are then min-max scaled between the range of  $[-1, 1]$ . Before infilling null values using one of the average, uniform or Gaussian distributions, or the proposed DLGN method, we store the null masks for each drug for the masked loss function.

Data	Metric	Trainset-Testset			Data	Metric	Trainset-Testset		
		Syn-Syn	Syn-Real	Real-Real			Syn-Syn	Syn-Real	Real-Real
Caco2	MSE	0.158	<b><u>0.131</u></b>	0.634	Half	MSE	0.248	<b><u>0.261</u></b>	0.525
	R2	-0.069	<b><u>0.137</u></b>	-3.215		R2	-0.320	<b><u>-0.275</u></b>	-1.589
	PCC	0.264	<b><u>0.426</u></b>	0.352		PCC	0.039	0.034	<b><u>0.156</u></b>
Lipo.	MSE	0.156	<b><u>0.150</u></b>	0.167	Cl. (H)	MSE	0.437	<b><u>0.433</u></b>	1.863
	R2	0.091	<b><u>0.138</u></b>	0.04		R2	-0.279	<b><u>-0.200</u></b>	-4.24
	PCC	0.368	0.409	<b><u>0.499</u></b>		PCC	0.053	0.096	<b><u>0.109</u></b>
AqSol	MSE	0.084	0.080	<b><u>0.075</u></b>	Cl. (M)	MSE	0.207	<b><u>0.209</u></b>	0.717
	R2	0.507	0.533	<b><u>0.564</u></b>		R2	-0.155	<b><u>-0.043</u></b>	-2.599
	PCC	0.713	0.731	<b><u>0.756</u></b>		PCC	0.173	<b><u>0.253</u></b>	0.132
FSolv	MSE	0.194	<b><u>0.165</u></b>	0.624	LD50	MSE	0.102	<b><u>0.100</u></b>	0.105
	R2	-0.139	<b><u>0.078</u></b>	-2.501		R2	0.253	<b><u>0.277</u></b>	0.240
	PCC	0.207	<b><u>0.391</u></b>	0.383		PCC	0.517	0.537	<b><u>0.542</u></b>
PPBR	MSE	0.270	<b><u>0.263</u></b>	3.527	hRG.1	MSE	0.126	<b><u>0.127</u></b>	0.136
	R2	-0.143	<b><u>-0.06</u></b>	-13.31		R2	-0.111	<b><u>-0.108</u></b>	-0.189
	PCC	0.162	<b><u>0.223</u></b>	0.095		PCC	0.060	0.062	0.062
VDss	MSE	0.201	<b><u>0.196</u></b>	0.535	hRG.10	MSE	0.115	<b><u>0.115</u></b>	0.121
	R2	-0.132	<b><u>-0.015</u></b>	-1.771		R2	-0.030	<b><u>-0.023</u></b>	-0.081
	PCC	0.206	<b><u>0.298</u></b>	0.234		PCC	0.189	0.196	<b><u>0.212</u></b>

Table 1: Comparing drug discovery regression performances between different combinations of augmented and real train sets, and augmented and real test sets. Values are averaged over 30 trials with the best scores on the real test set bolded. Statistical significance (underlined) is computed with a two-tailed T-test. Hyphenated pairs correspond to the train and test set used in the experiment.

## 4 Experiments

Below we describe model training details and compare our synthetic data to real data, in terms of machine learning efficiency (MLE) and univariate and bivariate statistical distributions. We then discuss ablation studies and key findings. Metrics for MLE, univariate, and bivariate evaluations are further defined in their respective subsections.

### 4.1 Training Details

Imagand Model		Diffusion Training	
Layers	12	Learning Rate	1e-3
Heads	16	Weight Decay	5e-2
MLP Dim.	768	Epoch	3000
Emb. Dropout	10%	Batch Size	256
Num Patches	48	Warmup	200
Cond. Emb. Size	768	Timesteps (Train)	2000
Time Emb. Size	64	Timesteps (Infer.)	150
PK Emb. Size	256	EMA Gamma ( $\gamma$ )	0.994

Table 2: List of Imagand Model Hyperparameters used across experiments. Model hyperparameters include the number of layers, heads, multilayered perceptron (MLP) size, embedding dropout, and sizes for the conditional, time, and pharmacokinetic (Y) embeddings. Training hyperparameters include the learning rate, weight decay, number of epochs, batch size, warmup, diffusion timesteps used for training and inference, and the Exponential Moving Average (EMA) Gamma ( $\gamma$ ).

We train a 19M parameter model for S2PK synthesis. Model hyperparameters were not optimized and are described in Table 2. We do not find overfitting to be an issue. For classifier-free guidance, we joint-train unconditionally via dropout zeroing out sections of the SMILES embeddings with 10% probability for all of our models. For the machine learning efficiency, and univariate and bivariate distribution analysis, we utilize DeBERTa embeddings trained on PubChem and DLGN for infilling and as the noise model. We compare our model configuration to other possible configurations in the ablation experiments. All experiments were conducted using a single NVIDIA GeForce RTX 3090 GPU.

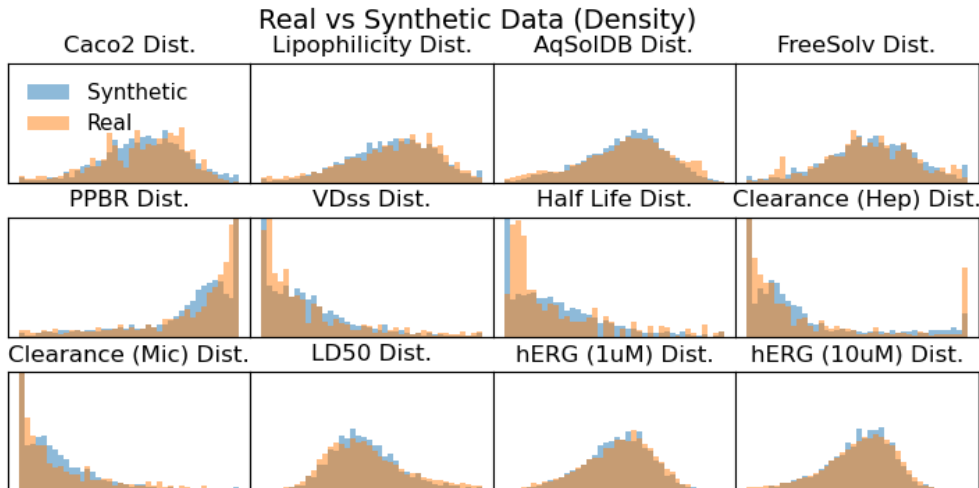


Figure 2: Distributions of ligand PK properties. Blue, synthetic distributions; orange, real distributions.

## 4.2 Machine Learning Efficiency

Using the trained S2PK model, we generate synthetic PK target properties for 3K ligands selected from our test dataset. The generated synthetic data, containing 3K ligands with all 12 target properties, can be used to augment real data for research requiring data spanning these target properties. Given the smaller size of real target property datasets, 3K synthetic target property ligands provide meaningful augmentations to the real data.

Machine Learning Efficiency (MLE) is a measure that assesses the ability of the synthetic data to replicate a specific use case [6, 7, 10]. MLE represents the ability of the synthetic data to replace or augment real data in downstream use cases. To measure MLE, two models are trained separately using synthetic versus real data, and then their performance, measured by mean-squared error, R2, and Pearson correlation coefficient, is evaluated on real data test sets and compared.

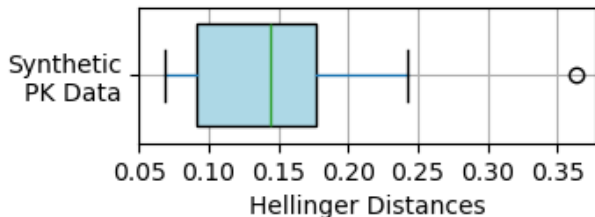


Figure 3: Synthetic PK Data Hellinger Distances (HDs).

For this experiment, we train Linear Regression (LR) models using ChemBERTa embeddings to predict each PK target property value. To prevent data leakage, we first divide real and synthetic data before combining them to form train and test sets, as follows. To ensure an adequately sized test set (>300 ligands, i.e. >10% size of our synthetic data) to evaluate our downstream models, we divide real data into segments denoted  $A_r$  and  $B_r$  using a 50%/50% split. To ensure a synthetic test set similar in size to real data test sets ( $\sim 300$  ligands), we divide synthetic data into segments denoted  $A_s$  and  $B_s$  using a 90%/10% split. The real train set is defined as  $A_r$  and the real test set is defined as  $B_r$ . The augmented train set is defined as  $A_r \cup A_s$  and the augmented test set is defined as  $B_r \cup B_s$ . Outliers are removed from both real and augmented train and test sets based on  $Q1 - 1.5IQR$  lower and  $Q3 + 1.5IQR$  upper bounds on the synthetic data.

Table 1 shows the results of the PK regression tasks using real and synthetic augmented datasets. Results of these experiments suggest that a synthetic augmented dataset can outperform real data with statistical significance over many PK datasets. Additional tasks will be explored in future work.

Data	Mean		Std	
	Real	Syn	Real	Syn
Caco2	0.118	0.137	0.388	0.375
Lipophilicity	0.184	0.179	0.417	0.386
AqSolDB	0.106	0.107	0.412	0.362
FreeSolv	0.103	0.123	0.421	0.400
PPBR	0.570	0.562	0.496	0.467
VDss	-0.603	-0.615	0.442	0.389
Half life	-0.557	-0.559	0.450	0.419
Clearance (H)	-0.549	-0.559	0.605	0.551
Clearance (M)	-0.670	-0.676	0.445	0.382
LD50	-0.038	-0.054	0.372	0.331
hERG 1uM	0.036	0.031	0.338	0.319
hERG 10uM	0.027	0.030	0.335	0.316

Table 3: Comparing mean and standard deviation values between real and synthetic target property values.

### 4.3 Univariate Distributions

The generated synthetic data closely matches that of the real data; see Figure 2. Hellinger distance (HD) quantifies the similarity between two probability distributions and can be used as a summary statistic of differences for each PK target property between real and synthetic datasets. Given two discrete probability distributions  $P = \{p_1, p_2, \dots, p_n\}$  and  $Q = \{q_1, q_2, \dots, q_n\}$ , the HD between  $P$  and  $Q$  is expressed in Equation 3.

$$HD^2(p, q) = \frac{1}{2} \sum_{i=1}^n (\sqrt{p_i} - \sqrt{q_i}) \quad (3)$$

With scores ranging between 0 to 1, HD values closer to 0 indicate smaller differences between real and synthetic data and are thus desirable. Figure 3 shows the HD values for our synthetic data compared to real data with the average HD being 0.15.

Table 3 compares the mean and standard deviation of the real and synthetic target property values. The mean and standard deviation of the generated synthetic data closely resemble that of the real data for each PK target property. We found that normalization combined with static thresholding substantially limits the generation of invalid and out-of-range PK values.

### 4.4 Bivariate Distributions

In addition to univariate comparisons, synthetic PK target properties can be compared to real data in terms of bivariate pairwise distributions and correlations. Bivariate pairwise scatterplots and Differential Pairwise Correlations (DPC) are shown in Figure 4. Many pairwise combinations of PK target properties have very few overlapping real data values, and pairwise combinations with fewer than 100 examples have their cardinality numbered in the heatmaps in Figure 4. We omit DPC values for pairwise combinations with cardinality less than 10.

In combination with univariate HD, DPC provides a multivariate metric for evaluating the quality of synthetic data when compared to real data. We define the DPC as the absolute difference between the bivariate correlation coefficient of real and synthetic data as shown in Equation 4.

$$\Delta CV_{cont_{XY}} = |\rho_{XY_r} - \rho_{XY_s}| \quad (4)$$

where  $X$  and  $Y$  denote the two continuous variables, whereas  $\rho_{XY}$  is the correlation coefficient for  $X$  and  $Y$ . If the real and synthetic PK target property datasets are highly similar (i.e., the synthetic dataset closely resembles the real dataset), then the absolute difference would be close to 0 or very small. Heatmap (b) in Figure 4 shows DPC on the Pearson correlation coefficient (PCC). The average DPC for PCC is 0.123. Heatmap (c) in Figure 4 shows DPC on the Spearman correlation coefficient (SCC). The average DPC for SCC is 0.138. These results indicate that the generated synthetic PK target properties resemble real data in pairwise correlations.

Many pairwise combinations of the real data have a small cardinality of  $< 100$ . As such, our synthetic PK target properties can benefit those pairwise combinations the most: researchers can augment pairwise real datasets with small cardinality to better answer pairwise target property research questions. Compared to pairwise target properties,

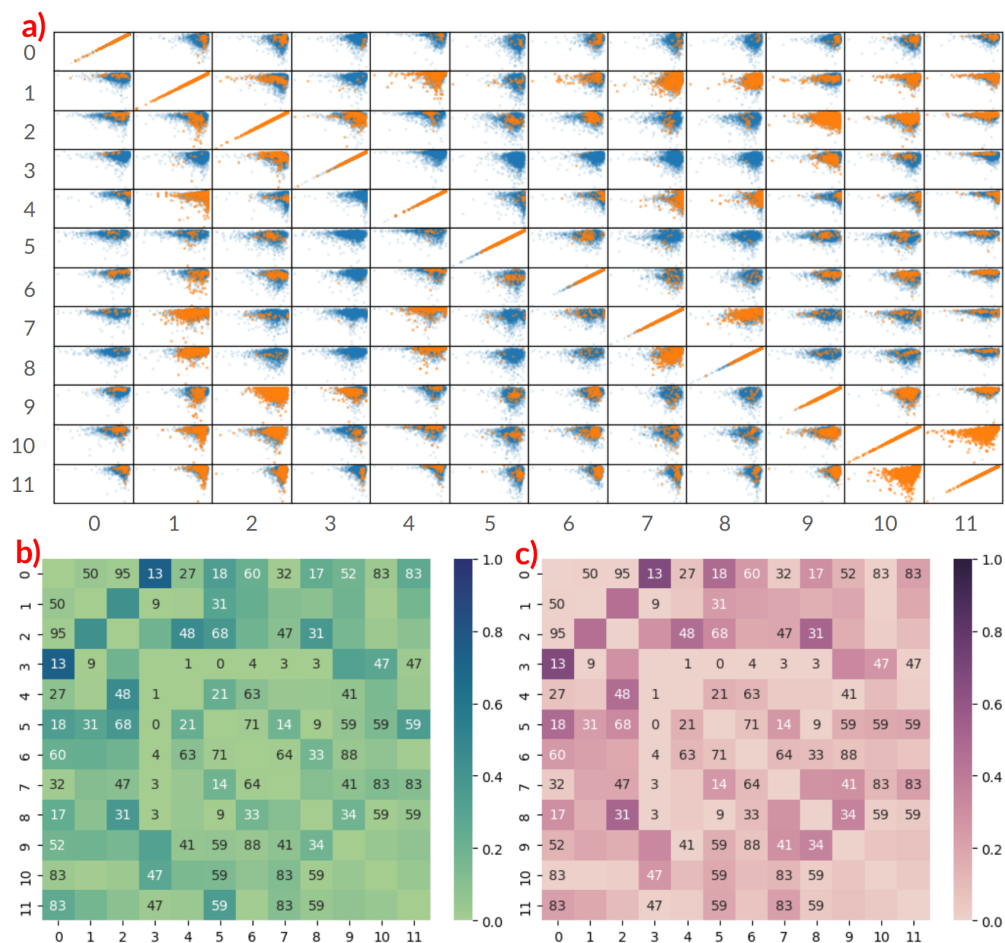


Figure 4: Overview of Bivariate Comparison Between Synthetic and Real Data. Graph (a) shows pairwise scatter plots for pairs of PK target properties. Real data is marked in orange and synthetic data is marked in blue. The heatmap plots (b) and (c) are the Differential Pairwise Correlations (DPC) for pairs of PK target properties between real and synthetic data. The heatmap (b) graphs the DPC for the Pearson correlation coefficient. The heatmap (c) graphs the DPC for the Spearman correlation coefficient. PK target property values are numbered in order of (0) Caco2, (1) Lipophilicity, (2) AQSolDB, (3) FreeSolv, (4) PPBR, (5) VDss, (6) Half Life, (7) Clearance (Hep), (8) Clearance (Mic), (9) LD50, (10) hERG (1uM), and (11) hERG (10uM).

overlap sparsity between combining multiple datasets results in even smaller cardinality. Scaling the S2PK model is straightforward, and can facilitate the generation of high-quality synthetic data that can be used to investigate multi-dataset research questions.

## 4.5 Ablation Studies

We conduct ablation studies to investigate the performance of our S2PK model given different SMILES encoders, encoder training sets, and sampling approaches for the infilling and noise model. Ablation study results (Table 4) are averages over 30 generated synthetic target property datasets, covering 90K target property values for ligands, for each ablation training run. Figure 5 graphs MSE between real and synthetic data generated during training for ablation experiments. From our ablation studies, we motivate our selected model configuration.

### 4.5.1 Pre-trained SMILES Encoder

We select different pre-trained SMILES encoders and pretraining datasets for ablation. Among encoder models, DeBERTa performs the best in terms of average HD and synthetic and real data MSE. Among encoder training datasets,



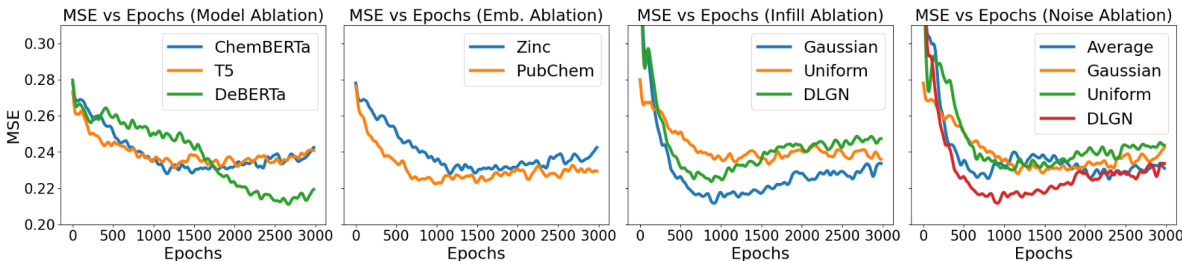


Figure 5: MSE between real and synthetic target property data generated during training for different ablation experiments.

Abl.	Exp	C2	Li	Aq	FS	PP	VD	HL	C.(H)	C.(M)	LD50	h.1	h.10	Avg
Model	CBrt	0.26	0.17	0.16	0.25	0.25	0.31	0.37	0.29	0.33	0.17	0.14	<b>0.13</b>	0.23
	DBrt	<b>0.21</b>	<b>0.16</b>	0.18	<b>0.20</b>	<b>0.22</b>	<b>0.27</b>	<b>0.36</b>	<b>0.24</b>	<b>0.28</b>	0.17	0.15	0.15	<b>0.21</b>
	T5	0.25	0.16	<b>0.15</b>	0.25	0.26	0.30	0.36	0.28	0.30	<b>0.15</b>	<b>0.13</b>	0.13	0.22
Emb.	Zinc	<b>0.26</b>	0.17	<b>0.16</b>	<b>0.25</b>	<b>0.25</b>	0.31	<b>0.37</b>	<b>0.29</b>	0.33	<b>0.17</b>	<b>0.14</b>	<b>0.13</b>	<b>0.23</b>
	PbC	0.27	<b>0.17</b>	0.16	0.25	0.27	<b>0.30</b>	0.38	0.30	<b>0.30</b>	0.17	0.15	0.15	0.24
Infill	Gau	<b>0.24</b>	<b>0.15</b>	<b>0.14</b>	<b>0.24</b>	<b>0.21</b>	<b>0.26</b>	<b>0.33</b>	<b>0.25</b>	0.25	<b>0.15</b>	<b>0.12</b>	<b>0.13</b>	<b>0.20</b>
	Uni	0.28	0.19	0.18	0.26	0.27	0.31	0.38	0.30	0.30	0.19	0.14	0.14	0.25
	DLG	0.26	0.16	0.15	0.25	0.23	0.29	0.36	0.27	<b>0.24</b>	0.16	0.13	0.13	0.22
Noise	Avg	<b>0.26</b>	<b>0.15</b>	0.22	0.28	0.25	0.39	0.39	0.28	0.33	0.18	0.15	0.16	0.25
	Gaus	0.26	0.17	0.16	<b>0.25</b>	0.25	0.31	0.37	0.29	0.33	0.17	<b>0.14</b>	<b>0.13</b>	0.23
	Unif	0.26	0.16	0.16	0.26	0.24	0.32	0.39	0.28	0.31	<b>0.16</b>	0.14	0.14	0.23
	DLG	0.27	0.18	<b>0.15</b>	0.26	<b>0.23</b>	<b>0.29</b>	<b>0.34</b>	<b>0.27</b>	<b>0.27</b>	0.16	0.14	0.14	<b>0.22</b>
<b>Our Model</b>		<u>0.19</u>	<u>0.12</u>	<u>0.13</u>	<u>0.18</u>	<u>0.20</u>	0.27	0.36	<u>0.20</u>	<u>0.19</u>	<u>0.11</u>	<u>0.09</u>	<u>0.09</u>	<u>0.18</u>

Table 4: Average Hellinger Distance Across 30 Generated Synthetic Target Property Datasets for Ablation Experiment Configurations. The best HD values for each ablation test are bolded. The best HD values across all ablation tests are underlined. HD values for our selected model configuration for MLE, univariate, and bivariate analysis are included in the table.

PubChem and Zinc have similar HD, with PubChem producing better synthetic and real data MSE. This motivates the choice of DeBERTa and PubChem for our selected model configuration.

#### 4.5.2 Discrete Local Gaussian Noise Model

We select different infilling strategies and noise models for ablation. Comparing noise model ablations, we measure the average MSE that each method injects into the data with Gaussian (1.19), uniform (0.53), and DLGN (0.29) ordered from most to least. This confirms that DLGN injects noise closely resembling the prior distribution. Similarly, we confirm DLGN has the best HD compared to Gaussian and uniform noise models. Comparing infilling ablations, DLGN has the best overall performance in HD and synthetic and real data MSE. This motivates the choice of DLGN for both infilling and noise models for our selected model configuration. In future work, we will explore additional noise techniques, such as quantile transformations.

## 5 Conclusions

The SMILES-to-Pharmacokinetic model Imagand generates synthetic PK target property data that closely resembles real data in univariate and bivariate distributions and for downstream tasks. Imagand provides a solution for the challenge of sparse overlapping PK target property data, allowing researchers to generate data to tackle complex research questions and for high-throughput screening. Future work will expand Imagand to categorical PK properties, and scale to more datasets and larger model sizes.

## References

- [1] Walid Ahmad, Elana Simon, Seyone Chithrananda, Gabriel Grand, and Bharath Ramsundar. Chemberta-2: Towards chemical foundation models. *arXiv preprint arXiv:2209.01712*, 2022.

- [2] Sameed Ahmed, Jennifer C Sullivan, and Anita T Layton. Impact of sex and pathophysiology on optimal drug choice in hypertensive rats: quantitative insights for precision medicine. *Iscience*, 24(4), 2021.
- [3] Jacob Austin, Daniel D Johnson, Jonathan Ho, Daniel Tarlow, and Rianne Van Den Berg. Structured denoising diffusion models in discrete state-spaces. *Advances in Neural Information Processing Systems*, 34:17981–17993, 2021.
- [4] Shekoofeh Azizi, Simon Kornblith, Chitwan Saharia, Mohammad Norouzi, and David J Fleet. Synthetic data from diffusion models improves imagenet classification. *arXiv preprint arXiv:2304.08466*, 2023.
- [5] Viraj Bagal, Rishal Aggarwal, PK Vinod, and U Deva Priyakumar. Molgpt: molecular generation using a transformer-decoder model. *Journal of Chemical Information and Modeling*, 62(9):2064–2076, 2021.
- [6] Mohammad Ahmed Basri, Bing Hu, Abu Yousuf Md Abdullah, Shu-Feng Tsao, Zahid Butt, and Helen Chen. A hyperparameter tuning framework for tabular synthetic data generation methods. *Journal of Computational Vision and Imaging Systems*, 9(1):76–79, 2023.
- [7] Vadim Borisov, Kathrin Seßler, Tobias Leemann, Martin Pawelczyk, and Gjergji Kasneci. Language models are realistic tabular data generators. *arXiv preprint arXiv:2210.06280*, 2022.
- [8] Nathan Brown, Marco Fiscato, Marwin H.S. Segler, and Alain C. Vaucher. Guacamol: Benchmarking models for de novo molecular design. *Journal of Chemical Information and Modeling*, 59(3):1096–1108, 2019. doi: 10.1021/acs.jcim.8b00839. URL <https://doi.org/10.1021/acs.jcim.8b00839>. PMID: 30887799.
- [9] Seyone Chithrananda, Gabriel Grand, and Bharath Ramsundar. Chemberta: Large-scale self-supervised pretraining for molecular property prediction, 2020.
- [10] Fida K Dankar and Mahmoud Ibrahim. Fake it till you make it: Guidelines for effective synthetic data generation. *Applied Sciences*, 11(5):2158, 2021.
- [11] Michael Davies, Rhys D.O. Jones, Ken Grime, Rasmus Jansson-Löfmark, Adrian J. Fretland, Susanne Winiwarter, Paul Morgan, and Dermot F. McGinnity. Improving the accuracy of predicted human pharmacokinetics: Lessons learned from the astrazeneca drug pipeline over two decades. *Trends in Pharmacological Sciences*, 41(6):390–408, 2020. ISSN 0165-6147. doi: <https://doi.org/10.1016/j.tips.2020.03.004>. URL <https://www.sciencedirect.com/science/article/pii/S0165614720300687>.
- [12] Prafulla Dhariwal and Alex Nichol. Diffusion models beat gans on image synthesis, 2021. URL <https://arxiv.org/abs/2105.05233>.
- [13] Li Di, Christopher Keefer, Dennis O Scott, Timothy J Strelevitz, George Chang, Yi-An Bi, Yurong Lai, Jonathon Duckworth, Katherine Fenner, Matthew D Troutman, et al. Mechanistic insights from comparing intrinsic clearance values between human liver microsomes and hepatocytes to guide drug design. *European journal of medicinal chemistry*, 57:441–448, 2012.
- [14] Alexey Dosovitskiy, Lucas Beyer, Alexander Kolesnikov, Dirk Weissenborn, Xiaohua Zhai, Thomas Unterthiner, Mostafa Dehghani, Matthias Minderer, Georg Heigold, Sylvain Gelly, Jakob Uszkoreit, and Neil Houlsby. An image is worth 16x16 words: Transformers for image recognition at scale, 2021. URL <https://arxiv.org/abs/2010.11929>.
- [15] Fang Du, Haibo Yu, Beiyan Zou, Joseph Babcock, Shunyou Long, and Min Li. hergcentral: a large database to store, retrieve, and analyze compound-human ether-a-go-go related gene channel interactions to facilitate cardiotoxicity assessment in drug development. *Assay and drug development technologies*, 9(6):580–588, 2011.
- [16] Vijay Prakash Dwivedi and Xavier Bresson. A generalization of transformer networks to graphs. *arXiv preprint arXiv:2012.09699*, 2020.
- [17] Anna Gaulton, Anne Hersey, Michał Nowotka, A Patricia Bento, Jon Chambers, David Mendez, Prudence Mutowo, Francis Atkinson, Louisa J Bellis, Elena Cibrián-Uhalte, et al. The chembl database in 2017. *Nucleic acids research*, 45(D1):D945–D954, 2017.
- [18] Zhiye Guo, Jian Liu, Yanli Wang, Mengrui Chen, Duolin Wang, Dong Xu, and Jianlin Cheng. Diffusion models in bioinformatics and computational biology. *Nature Reviews Bioengineering*, pages 1–19, 2023.
- [19] Pengcheng He, Xiaodong Liu, Jianfeng Gao, and Weizhu Chen. Deberta: Decoding-enhanced bert with disentangled attention, 2021. URL <https://arxiv.org/abs/2006.03654>.
- [20] Jonathan Ho and Tim Salimans. Classifier-free diffusion guidance, 2022. URL <https://arxiv.org/abs/2207.12598>.
- [21] Jonathan Ho, Ajay Jain, and Pieter Abbeel. Denoising diffusion probabilistic models, 2020.
- [22] Jonathan Ho, Chitwan Saharia, William Chan, David J. Fleet, Mohammad Norouzi, and Tim Salimans. Cascaded diffusion models for high fidelity image generation, 2021. URL <https://arxiv.org/abs/2106.15282>.

- [23] Jonathan Ho, Tim Salimans, Alexey Gritsenko, William Chan, Mohammad Norouzi, and David J. Fleet. Video diffusion models, 2022. URL <https://arxiv.org/abs/2204.03458>.
- [24] Emiel Hooeboom, Victor Garcia Satorras, Clément Vignac, and Max Welling. Equivariant diffusion for molecule generation in 3d, 2022.
- [25] Bing Hu, Ashish Saragadam, Anita Layton, and Helen Chen. Synthetic data from diffusion models improve drug discovery prediction, 2024. URL <https://arxiv.org/abs/2405.03799>.
- [26] Han Huang, Leilei Sun, Bowen Du, and Weifeng Lv. Conditional diffusion based on discrete graph structures for molecular graph generation, 2023.
- [27] Kexin Huang, Tianfan Fu, Wenhao Gao, Yue Zhao, Yusuf Roohani, Jure Leskovec, Connor W. Coley, Cao Xiao, Jimeng Sun, and Marinka Zitnik. Therapeutics data commons: Machine learning datasets and tasks for drug discovery and development, 2021.
- [28] Ilia Igashov, Hannes Stärk, Clément Vignac, Victor Garcia Satorras, Pascal Frossard, Max Welling, Michael Bronstein, and Bruno Correia. Equivariant 3d-conditional diffusion models for molecular linker design, 2022.
- [29] John J Irwin and Brian K Shoichet. Zinc- a free database of commercially available compounds for virtual screening. *Journal of chemical information and modeling*, 45(1):177–182, 2005.
- [30] Jintae Kim, Sera Park, Dongbo Min, and Wankyung Kim. Comprehensive survey of recent drug discovery using deep learning. *International Journal of Molecular Sciences*, 22(18):9983, 2021.
- [31] Sunghwan Kim, Jie Chen, Tiejun Cheng, Asta Gindulyte, Jia He, Siqian He, Qingliang Li, Benjamin A Shoemaker, Paul A Thiessen, Bo Yu, et al. Pubchem 2023 update. *Nucleic acids research*, 51(D1):D1373–D1380, 2023.
- [32] I Kola. The state of innovation in drug development. *Clinical pharmacology and therapeutics*, 83:227–30, 02 2008. doi: 10.1038/sj.cpt.6100479.
- [33] Majun Lian, Wenli Du, Xinjie Wang, and Qian Yao. Drug-target interaction prediction based on multi-similarity fusion and sparse dual-graph regularized matrix factorization. *IEEE Access*, 9:99718–99730, 2021.
- [34] Franco Lombardo and Yankang Jing. In silico prediction of volume of distribution in humans. extensive data set and the exploration of linear and nonlinear methods coupled with molecular interaction fields descriptors. *Journal of chemical information and modeling*, 56(10):2042–2052, 2016.
- [35] David L Mobley and J Peter Guthrie. Freesolv: a database of experimental and calculated hydration free energies, with input files. *Journal of computer-aided molecular design*, 28:711–720, 2014.
- [36] Deisy Morselli Gysi, Italo do Valle, Marinka Zitnik, Asher Ameli, Xiao Gan, Onur Varol, Susan Dina Ghiassian, J. J. Patten, Robert A. Davey, Joseph Loscalzo, and Albert-Laszlo Barabasi. Network medicine framework for identifying drug-repurposing opportunities for covid-19. *Proceedings of the National Academy of Sciences*, 118 (19), April 2021. ISSN 1091-6490. doi: 10.1073/pnas.2025581118. URL <http://dx.doi.org/10.1073/pnas.2025581118>.
- [37] David P Nusinow, John Szpyt, Mahmoud Ghandi, Christopher M Rose, E Robert McDonald, Marian Kalocsay, Judit Jané-Valbuena, Ellen Gelfand, Devin K Schweppe, Mark Jedrychowski, et al. Quantitative proteomics of the cancer cell line encyclopedia. *Cell*, 180(2):387–402, 2020.
- [38] R Scott Obach, Franco Lombardo, and Nigel J Waters. Trend analysis of a database of intravenous pharmacokinetic parameters in humans for 670 drug compounds. *Drug Metabolism and Disposition*, 36(7):1385–1405, 2008.
- [39] Olga Obrezanova. Artificial intelligence for compound pharmacokinetics prediction. *Current Opinion in Structural Biology*, 79:102546, 2023.
- [40] Maryam Pouryahya, Jung Hun Oh, James C Mathews, Zehor Belkhatir, Caroline Moosmüller, Joseph O Deasy, and Allen R Tannenbaum. Pan-cancer prediction of cell-line drug sensitivity using network-based methods. *International Journal of Molecular Sciences*, 23(3):1074, 2022.
- [41] Sudeep Pushpakom, Francesco Iorio, Patrick A Eyers, K Jane Escott, Shirley Hopper, Andrew Wells, Andrew Doig, Tim Williams, Joanna Latimer, Christine McNamee, et al. Drug repurposing: progress, challenges and recommendations. *Nature reviews Drug discovery*, 18(1):41–58, 2019.
- [42] Colin Raffel, Noam Shazeer, Adam Roberts, Katherine Lee, Sharan Narang, Michael Matena, Yanqi Zhou, Wei Li, and Peter J. Liu. Exploring the limits of transfer learning with a unified text-to-text transformer, 2023. URL <https://arxiv.org/abs/1910.10683>.
- [43] Jennifer E. Sager, Jingjing Yu, Isabelle Ragueneau-Majlessi, and Nina Isoherranen. Physiologically based pharmacokinetic (pbpk) modeling and simulation approaches: A systematic review of published models, applications, and model verification. *Drug Metabolism and Disposition*, 43(11):1823–1837, 2015. ISSN 0090-9556. doi: 10.1124/dmd.115.065920. URL <https://dmd.aspetjournals.org/content/43/11/1823>.

- [44] Chitwan Saharia, William Chan, Saurabh Saxena, Lala Li, Jay Whang, Emily Denton, Seyed Kamyar Seyed Ghasemipour, Burcu Karagol Ayan, S. Sara Mahdavi, Rapha Gontijo Lopes, Tim Salimans, Jonathan Ho, David J Fleet, and Mohammad Norouzi. Photorealistic text-to-image diffusion models with deep language understanding, 2022.
- [45] Victor Garcia Satorras, Emiel Hooeboom, Fabian B. Fuchs, Ingmar Posner, and Max Welling. E(n) equivariant normalizing flows for molecule generation in 3d. *CoRR*, abs/2105.09016, 2021. URL <https://arxiv.org/abs/2105.09016>.
- [46] Silvia Scoarta, Asli Küçükosmanoglu, Felix Bindt, Marianne Pouwer, and Bart A. Westerman. Review: A roadmap to use nonstructured data to discover multitarget cancer therapies. *JCO Clinical Cancer Informatics*, 7:e2200096, 2023. doi: 10.1200/CCI.22.00096. URL <https://doi.org/10.1200/CCI.22.00096>. PMID: 37116097.
- [47] Murat Cihan Sorkun, Abhishek Khetan, and Süleyman Er. Aqsoldb, a curated reference set of aqueous solubility and 2d descriptors for a diverse set of compounds. *Scientific data*, 6(1):143, 2019.
- [48] Nitish Srivastava, Geoffrey Hinton, Alex Krizhevsky, Ilya Sutskever, and Ruslan Salakhutdinov. Dropout: A simple way to prevent neural networks from overfitting. *Journal of Machine Learning Research*, 15(56):1929–1958, 2014. URL <http://jmlr.org/papers/v15/srivastava14a.html>.
- [49] Antti Tarvainen and Harri Valpola. Mean teachers are better role models: Weight-averaged consistency targets improve semi-supervised deep learning results, 2018. URL <https://arxiv.org/abs/1703.01780>.
- [50] Maha A Thafar, Mona Alshahrani, Somayah Albaradei, Takashi Gojobori, Magbubah Essack, and Xin Gao. Affinity2vec: drug-target binding affinity prediction through representation learning, graph mining, and machine learning. *Scientific reports*, 12(1):4751, 2022.
- [51] Ashish Vaswani, Noam Shazeer, Niki Parmar, Jakob Uszkoreit, Llion Jones, Aidan N. Gomez, Lukasz Kaiser, and Illia Polosukhin. Attention is all you need, 2023. URL <https://arxiv.org/abs/1706.03762>.
- [52] Clement Vignac, Igor Krawczuk, Antoine Siraudin, Bohan Wang, Volkan Cevher, and Pascal Frossard. Digress: Discrete denoising diffusion for graph generation, 2023.
- [53] Ning-Ning Wang, Jie Dong, Yin-Hua Deng, Minfeng Zhu, Ming Wen, Zhiqiang Yao, Aiping Lu, Jian bing Wang, and Dongsheng Cao. Adme properties evaluation in drug discovery: Prediction of caco-2 cell permeability using a combination of nsga-ii and boosting. *Journal of chemical information and modeling*, 56 4:763–73, 2016. URL <https://api.semanticscholar.org/CorpusID:206609089>.
- [54] Sheng Wang, Yuzhi Guo, Yuhong Wang, Hongmao Sun, and Junzhou Huang. Smiles-bert: Large scale unsupervised pre-training for molecular property prediction. *Proceedings of the 10th ACM International Conference on Bioinformatics, Computational Biology and Health Informatics*, 2019. URL <https://api.semanticscholar.org/CorpusID:202159174>.
- [55] Michael J. Waring, John Edmund Arrowsmith, Andrew R. Leach, Paul D. Leeson, Sam Mandrell, Robert M. Owen, Garry Pairaudeau, William D. Pennie, Stephen D. Pickett, Jibo Wang, Owen Wallace, and Alexander Weir. An analysis of the attrition of drug candidates from four major pharmaceutical companies. *Nature Reviews Drug Discovery*, 14:475–486, 2015. URL <https://api.semanticscholar.org/CorpusID:25292436>.
- [56] Mark Wenlock and Nicholas Tomkinson. Experimental in vitro dmpk and physicochemical data on a set of publicly disclosed compounds. *CHEMBL*, 2016. doi: 10.6019/CHEMBL3301361.
- [57] Thomas Wolf, Lysandre Debut, Victor Sanh, Julien Chaumond, Clement Delangue, Anthony Moi, Pierric Cistac, Tim Rault, Rémi Louf, Morgan Funtowicz, Joe Davison, Sam Shleifer, Patrick von Platen, Clara Ma, Yacine Jernite, Julien Plu, Canwen Xu, Teven Le Scao, Sylvain Gugger, Mariama Drame, Quentin Lhoest, and Alexander M. Rush. Transformers: State-of-the-art natural language processing. In *Proceedings of the 2020 Conference on Empirical Methods in Natural Language Processing: System Demonstrations*, pages 38–45, Online, October 2020. Association for Computational Linguistics. URL <https://www.aclweb.org/anthology/2020.emnlp-demos.6>.
- [58] Lemeng Wu, Chengyue Gong, Xingchao Liu, Mao Ye, and Qiang Liu. Diffusion-based molecule generation with informative prior bridges, 2022.
- [59] Zhenqin Wu, Bharath Ramsundar, Evan N Feinberg, Joseph Gomes, Caleb Geniesse, Aneesh S Pappu, Karl Leswing, and Vijay Pande. Moleculenet: a benchmark for molecular machine learning. *Chemical science*, 9(2): 513–530, 2018.
- [60] Hao Zhu, Todd M Martin, Lin Ye, Alexander Sedykh, Douglas M Young, and Alexander Tropsha. Quantitative structure- activity relationship modeling of rat acute toxicity by oral exposure. *Chemical research in toxicology*, 22(12):1913–1921, 2009.

- [61] Marinka Žitnik, Edward A Nam, Christopher Dinh, Adam Kuspa, Gad Shaulsky, and Blaž Zupan. Gene prioritization by compressive data fusion and chaining. *PLoS computational biology*, 11(10):e1004552, 2015.